STRUCTURE FABRICATION AND CONTROL OF HIGHER ORDER MODES

A. Marziali and H. A. Schwettman

W. W. Hansen Experimental Physics Laboratory

Stanford University

Stanford, CA 94305-4085

J.G.Hatmaker

Babcock & Wilcox, a McDermott Company

Accelerator Structures

P.O. Box 785, Lynchburg, VA 24505

ABSTRACT

Loading of higher order modes in superconducting multi-cell structures is complicated by field profile errors caused by current fabrication techniques and procedures. A 1300 MHz CERN/DESY structure has been fabricated using modified techniques and procedures. It appears that these eliminate the need for post-fabrication tuning to achieve a flat field profile in the accelerator mode and, in addition, provide good control of the field profile in the Higher Order Modes. The fabrication procedure is described and the resulting field profiles for a 1300 MHz two-cell structure are evaluated.

1. INTRODUCTION

The manufacturing techniques and fabrication procedures currently being used in the construction of superconducting multi-cell structures are less precise than those used in room temperature structures. Superconducting structures typically have been manufactured to low tolerance and individual cells have then been deformed to flatten the accelerator mode field profile and achieve the correct resonant frequency. This philosophy decreases production costs, but it also increases the risk that control of Higher Order Modes (HOMs) will be lost. In the mid-1980's one of us (H.A.S.) reviewed RF measurements of four-cell structures at CERN and DESY and found that the external loading of HOMs with large impedance varied from structure to structure by as much as a factor of three, and the loading of HOMs with small impedance varied by as much as an order of magnitude. While part of this variation might be attributed to variation in the HOM couplers themselves, the principal cause is most likely the variation in field profile of the HOMs. Field profile problems will increase as one proceeds from four cell structures to structures of seven or nine cells.

We have recently constructed a 1300 MHz two-cell version of the CERN/DESY structure[1][2]. We selected manufacturing techniques and fabrication procedures that result in improved dimensional tolerances and better control of HOMs. The most important modes

of the two-cell structure and the techniques and procedures used in the fabrication of this structure are discussed in Sections 2 and 3 of this paper. Mechanical and RF measurements on the principal structure components (dumbbell and end half-cells with beam tube) are described in Section 4. In Section 5 and 6, RF measurements on the completed two-cell CERN/DESY structure are described and the results evaluated.

2. STRUCTURE MODES

The lowest frequency longitudinal and dipole modes of the two-cell CERN/DESY structure, calculated using URMEL[3], are listed in Table 1. As shown in Figure 1, the beam tube in the CERN/DESY structure has a section of expanded diameter and a section of reduced diameter. The cutoff frequencies of the TM_{01} and the TE_{11} modes in both the expanded and reduced beam tube sections are also listed in the table.
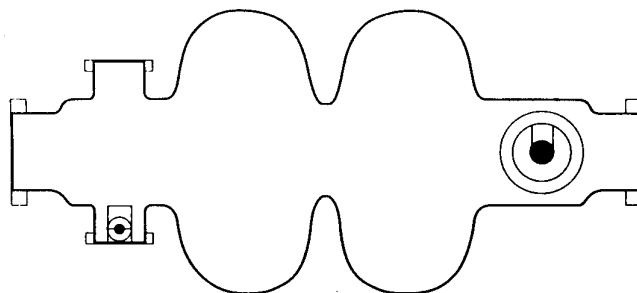
1300 MHz TWO CELL STRUCTURE

Figure 1: CERN/DESY 1300 MHz two-cell structure with beam tubes. Beam tube ports are rotated to the view plane for clarity.

TABLE 1: URMEL CALCULATED MODES FOR TWO-CELL STRUCTURE

LONGITUDINAL MODES

Mode	Comments		Freq. (MHz)	R/Q (Ω)	$\delta f/\delta E$
0-EE-1	"TM_{010}"	0 mode	1287.31	0.001	.0091
0-ME-1	"TM_{010}"	π mode	1298.30	115.22	.0089
0-EE-2	"TM_{011}"	π mode	2321.44	2.773	.013
0-ME-2	"TM_{011}"	0 mode	2354.18	36.405	.0093
0-EE-3	"TM_{020}"	0 mode	2698.93	0.052	.018
0-ME-3	"TM_{020}"	π mode	2739.13	0.721	.017
TM_{01} cutoff (expanded sect.)			2958	–	
0-EE-4	Beam tube 0 mode		3160.02	0.004	
0-ME-4	Beam tube π mode		3165.82	3.122	
TM_{01} cutoff (reduced sect.)			4272	–	

DIPOLE MODES

Mode	Comments		Freq. (MHz)	(R/Q)' (Ω)	$\delta f/\delta E$
1-ME-1	"TE_{111}"	0 mode	1649.88	4.243	.0439
1-EE-1	"TE_{111}"	π mode	1712.96	8.216	.0422
1-ME-2	"TM_{110}"	π mode	1838.63	15.748	.093
1-EE-2	"TM_{110}"	0 mode	1895.44	6.721	.032
TE_{11} cutoff (expanded sect.)			2263	–	
1-ME-3	Beam tube 0 mode		2433.02	1.150	
1-EE-3	Beam tube π mode		2441.11	0.149	
1-ME-4			2546.73	10.589	
1-EE-4			2776.98	0.407	
1-ME-5			2827.07	0.537	
1-EE-5			2937.44	0.085	
1-ME-6			3017.72	1.295	
1-EE-6	"Trapped" mode		3066.33	0.223	.067
TE_{11} cutoff (reduced sect.)			3268	–	

The lowest frequency longitudinal modes, as expected, are the "TM_{010}", the "TM_{011}", and the "TM_{020}" modes. All of these modes are reasonably well confined to the cell region of the structure. The fourth band of longitudinal modes appears at 3160 MHz to 3166 MHz, a frequency beyond cutoff for the expanded beam tube section. If we model the expanded beam tube as a cylindrical resonator with an electric boundary at the reducing transition and a magnetic boundary at the entrance to the cell, the TM_{011} mode frequency is analytically calculated to be 3098 MHz. The URMEL calculated field profile confirms that this fourth longitudinal mode is the "TM_{011}" resonance of the expanded beam tube.

The lowest frequency dipole modes are the "TE_{111}" and "TM_{110}" modes. Again, both of these modes are reasonably well confined to the cell region of the structure. The third band of dipole modes appears at 2433 MHz to 2441 MHz, beyond the TE_{11} cutoff for the expanded beam tube section. If we perform an analysis similar to that for the TM_{011} mode, we find that the TE_{111} mode frequency in the expanded beam tube is 2441 MHz. URMEL calculated fields once again confirm that this third dipole mode is the "TE_{111}" resonance of the expanded beam tube region.

As indicated in the table, there are a number of other dipole modes at frequencies below the TE_{11} cutoff (reduced section) at 3268 MHz; among these, the mode 1-EE-6 at 3066 MHz deserves

special mention. This is the well known "trapped" dipole mode
for which URMEL calculations indicate very small field amplitude
in the beam tubes.

Using URMEL, we have also calculated the field unflatness
resulting from a given cell frequency error in a two-cell cavity.
This ratio $\delta f/\delta E$ (percent frequency difference / percent field
difference) is listed in the table for the most important modes.

3. TECHNIQUES AND PROCEDURES

The manufacturing techniques and fabrication procedures used for
the 1300 MHz CERN/DESY structures have been described in some
detail elsewhere[4]. Both the half cells and the beam tubes were
formed by deep drawing and the structure components were then
joined by electron beam welding. Interlocking joints were
provided for each weld. Assembly of the structure proceeded by
completing the iris weld between half cells to form a dumbbell
and by welding the end half cells to the beam tubes. The equator
welds were made subsequently. This fabrication sequence was
adopted because welding in the iris region of the structure is
the most difficult to control; given this sequence, it is
possible to make both dimensional and RF measurements on the
dumbbells and the end-cells with beam tube before proceeding to
the final welding at the cell equators. Also, this fabrication

807

procedure allows access to the iris welds for dressing or polishing of the weld.

With the manufacturing techniques employed, we felt it was reasonable to expect dimensional tolerances of a few mils (1 mil = .001 inch) in fabrication of the dumbbells and the end half-cells with beam tube. On this basis one might expect that half-cell frequencies would be reproducible to within $\pm$ 5 X 10^{-4} ($\pm$ 650 kHz) and that cell-to-cell coupling coefficients would be reproducible to within a few percent. To check this assumption, dimensional measurements have been made on four dumbbells using a Zeiss computerized coordinate measuring machine (CMM). The CMM scanned the inside profile of each half-cell at four different azimuthal angles and calculated the error at each point as a perpendicular displacement from a reference geometry. For the first dumbbell manufactured, deviations from the reference profile as large as 20 mils are observed as can be seen in Figure 2. However, variations in cell geometry, as opposed to deviation from the reference, are always less than $\pm$ 10 mils. Often, the largest error is at the iris and can be corrected. Since the dumbbell shown in Figure 2 was the worst fabricated, we chose to use it in the two-cell structure.
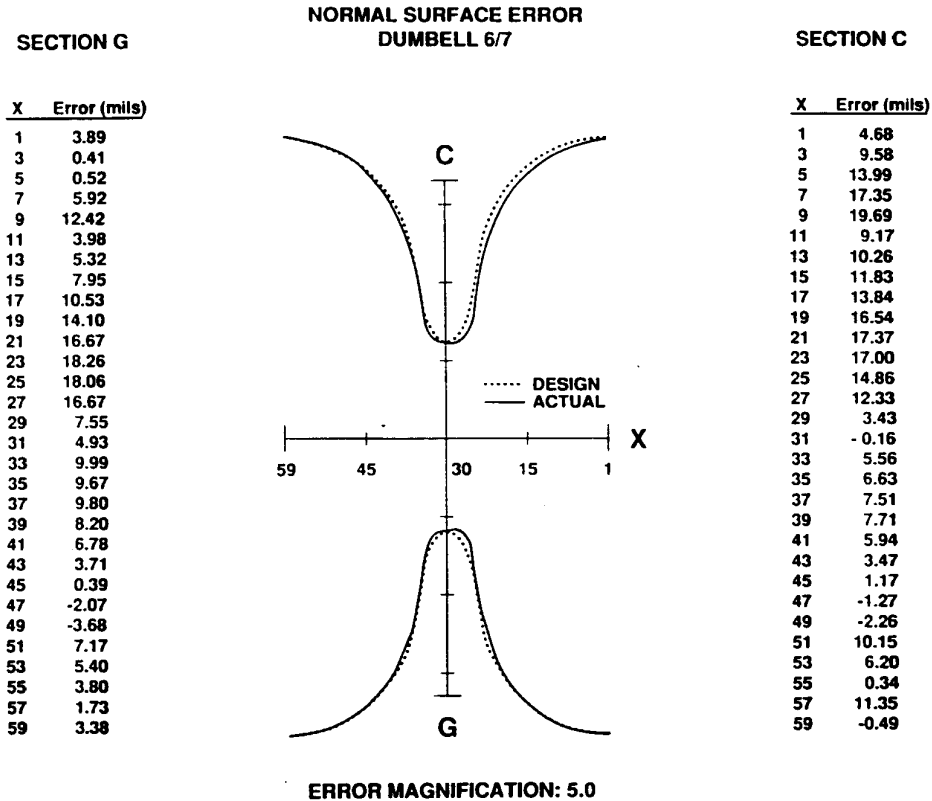
NORMAL SURFACE ERROR
DUMBELL 6/7

SECTION G				SECTION C	
X	**Error (mils)**			**X**	**Error (mils)**
1	3.89			1	4.68
3	0.41			3	9.58
5	0.52			5	13.99
7	5.92			7	17.35
9	12.42			9	19.69
11	3.98			11	9.17
13	5.32			13	10.26
15	7.95			15	11.83
17	10.53			17	13.84
19	14.10			19	16.54
21	16.67			21	17.37
23	18.26			23	17.00
25	18.06			25	14.86
27	16.67			27	12.33
29	7.55			29	3.43
31	4.93			31	- 0.16
33	9.99			33	5.56
35	9.67			35	6.63
37	9.80			37	7.51
39	8.20			39	7.71
41	6.78			41	5.94
43	3.71			43	3.47
45	0.39			45	1.17
47	-2.07			47	-1.27
49	-3.68			49	-2.26
51	7.17			51	10.15
53	5.40			53	6.20
55	3.80			55	0.34
57	1.73			57	11.35
59	3.38			59	-0.49

C

······ DESIGN
—— ACTUAL

59   45   30   15   1   X

G

ERROR MAGNIFICATION: 5.0

Figure 2: Zeiss CMM profile of a section of dumbbell 6/7.

For the accelerator mode it is our objective to control the
frequencies of individual cells to within $\pm$ 5 X 10^{-5} ($\pm$ 65 kHz),
a spread one order of magnitude smaller than the expected
manufacturing tolerances for dumbbells and for end half-cells
with beam tube. This level of control is adequate to achieve a
flat field profile even in structures of seven to nine cells. It
is also possible that a procedure designed to correct cell
frequency errors in the accelerator mode will be partially
successful in correcting errors in the HOMs. A reasonable

approach to this correction problem is to make RF measurements and use these to guide a fine tuning procedure. There are at least three options. One can complete the equator welds, make RF measurements on the assembled structure, and then deform individual cells to achieve a flat field profile. Alternatively one can use RF measurements on the components to guide a tuning procedure that could either be uniform removal of material (chemically) from the interior cell wall, or adjustment of half-cell length by machining. If either of the last two options is adopted, then for a 1300 MHz structure one must control the contraction of the final equator weld to within $\pm$ 1 mil.

A priori, it is simply not possible to determine whether one of these options is better than another. Nonetheless, it may be instructive to point out some consequences of tuning individual cells by $\pm$ 5 X 10^{-4} ($\pm$ 650 kHz). If one proceeds with the deformation option, one must compress or extend single cells by $\pm$ 13.5 mils. If one proceeds with chemical removal of material, then the interior surface of the cells will vary by $\pm$ 2 mils. And if one proceeds with adjustment of cell length by machining, the cell lengths will differ by $\pm$ 10 mils. Although these numbers led us to express a preference[4] for chemical tuning, the two-cell structure described in this paper was, in fact, tuned by cell length machining.

4. RF MEASUREMENTS ON STRUCTURE COMPONENTS

RF measurements were made on four dumbbells and four end half-cells with beam tube. These structure components were subsequently assembled into a two-cell structure and a four-cell structure. All RF measurements were made at a temperature of 68° F with the structure components filled to a pressure of one atmosphere with dry nitrogen. The dumbbells and the end half-cells with beam tube both were terminated with brass plates that served as electrical shorts across the equatorial plane.

Since the structure components were fabricated with a very precise incremental length at the equator, RF measurements could be used directly to assess reproducibility. In Table 2 the "TM_{010}" mode frequencies of the four end cells with beam tube are listed. It is evident that the frequencies fall within ± 360 kHz, a range somewhat smaller than our expected fabrication tolerances.

TABLE 2: FREQUENCIES OF END HALF-CELLS WITH BEAM TUBE

End-cell	freq. (MHz)
XB001	1287.37
XB002	1286.65
XB003	1287.33
XB006	1286.72

For each of the four dumbbells, we have determined both the

coupling coefficients and half-cell frequencies. The coupling
coefficients γ were calculated from the measured 0-mode and π-
mode frequencies of each dumbbell:

$$\gamma = 2 \frac{f_\pi - f_0}{f_\pi + f_0}$$

Eqn. (1)

Using a simple equivalent circuit and perturbation theory[5] the
frequencies of the two half-cells were calculated from the
measured on-axis electric field profile in either the 0-mode or
π-mode of the dumbbell. For a dumbbell the perturbation theory
equations reduce to:

$$\frac{\delta \omega}{\omega}\bigg|_\pi = \gamma \langle I_0, I_\pi' \rangle (-1)^m$$

Eqn. (2)

$$\frac{\delta \omega}{\omega}\bigg|_0 = \gamma \langle I_\pi, I_0' \rangle (-1)^m$$

Eqn. (3)

where m = 0,1 is the cell number. The vectors I_β are the
calculated modes in the form of two element normalized vectors.
The measured field profiles I_β' also consist of normalized two
element vectors, where each element is the peak on-axis field in
one half-cell. To measure the field profiles, a dielectric bead
is pulled on axis through the dumbbell while the shift in the
resonant frequency is recorded. The relative electric field
profile is then obtained by taking the square root of the
frequency perturbation caused by the bead.

The frequencies of the two half-cells and the coupling
coefficients for each dumbbell are listed in Table 3. It can be

seen that the eight half-cell frequencies all lie within ± 650
kHz of each other. Excluding the first dumbbell manufactured
(6/7), the coupling coefficients fall within ± 1.5 percent of
each other.

TABLE 3:   DUMBBELL HALF-CELL FREQUENCIES AND COUPLING COEFFICIENT

Dumbbell cell 1/2	freq. (MHz) cell 1	freq. (MHz) cell 2	Coupling coefficient
11 / 12	1277.84	1278.27	.0181
13 / 14	1278.68	1277.55	.0177
15 / 16	1278.05	1278.81	.0176
6 / 7	1278.23	1278.60	.0171

5. EVALUATION OF STRUCTURE

The manufacturing techniques and fabrication procedures outlined
in the previous section have been evaluated by measuring the
field profiles in all of the lower frequency modes of the
completed two-cell structure. Field profile measurements have
been made on the structure as fabricated and have been
interpreted using the URMEL calculations described in Section 2.

5.1 Lowest frequency modes confined to the cells.

In Figure 3, the 0-mode and π-mode field profiles for the first
three longitudinal bands are presented. The field profiles for
the "TM_{010}" band are flat to within 0.3 percent. Using this field
error and the URMEL parameter, the frequency difference between

LOWEST FREQUENCY RF LONGITUDINAL MODES
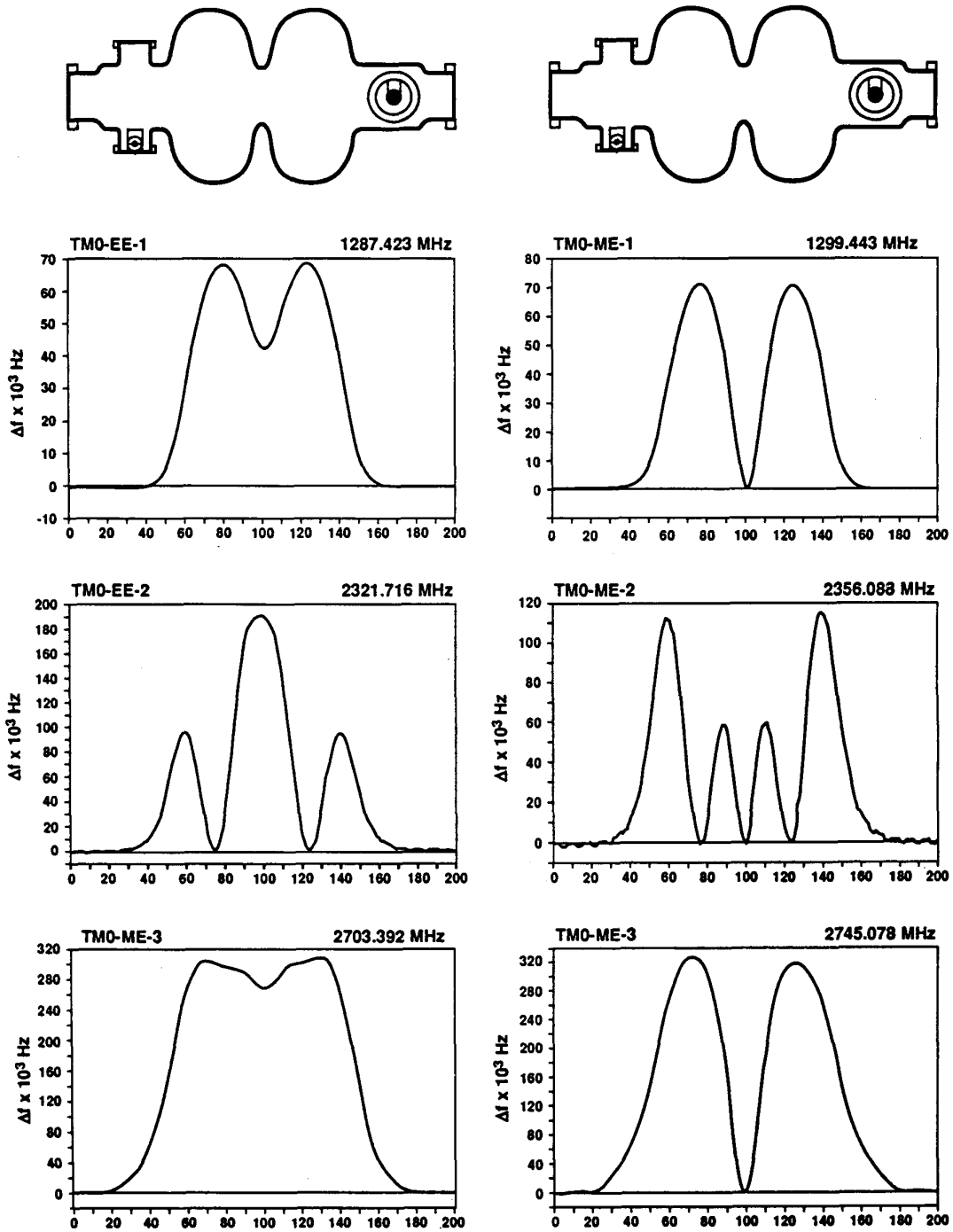
Figure 3: Field profiles for the lowest frequency longitudinal modes.

the two cells is calculated to be 2×10^{-5} of the average frequency. Based on the expected variation in weld shrinkage at the equator ($\pm$ 1 mil), one might have expected a frequency variation of $\pm 5 \times 10^{-5}$.

The 0-mode and π-mode field profiles for the "TM_{011}" band and the "TM_{020}" band present a similar, yet somewhat different picture. The field amplitude difference for both these modes is 1.5 percent, and the URMEL analysis yields a frequency difference of 2×10^{-4} between cells in the π-mode and 1.4×10^{-4} between the cells in the 0-mode. These frequency differences are larger than for the accelerator mode, but smaller than the $\pm 5 \times 10^{-4}$ variation one might expect based on the dumbbell manufacturing tolerances. This result suggests that the procedure used to correct errors in the accelerator mode is partially successful in correcting errors in the HOMs.

Similar behavior is observed in the dipole modes. The 0-mode and π-mode field profile for the "TE_{111}" band and the "TM_{110}" band are shown in Figure 4. For the "TE_{111}" band the measured field difference is 1 percent for the π-mode, leading to an URMEL calculated cell frequency difference of 4×10^{-4}, while for the 0-mode the field error is 1.5 percent and the cell frequency difference is 7×10^{-4}. For the "TM_{110}" modes the field error is 0.5 percent for the 0-mode and < 1.5 percent for the π-mode. In the 0-mode the cell frequency difference is 2×10^{-4}. In the π-

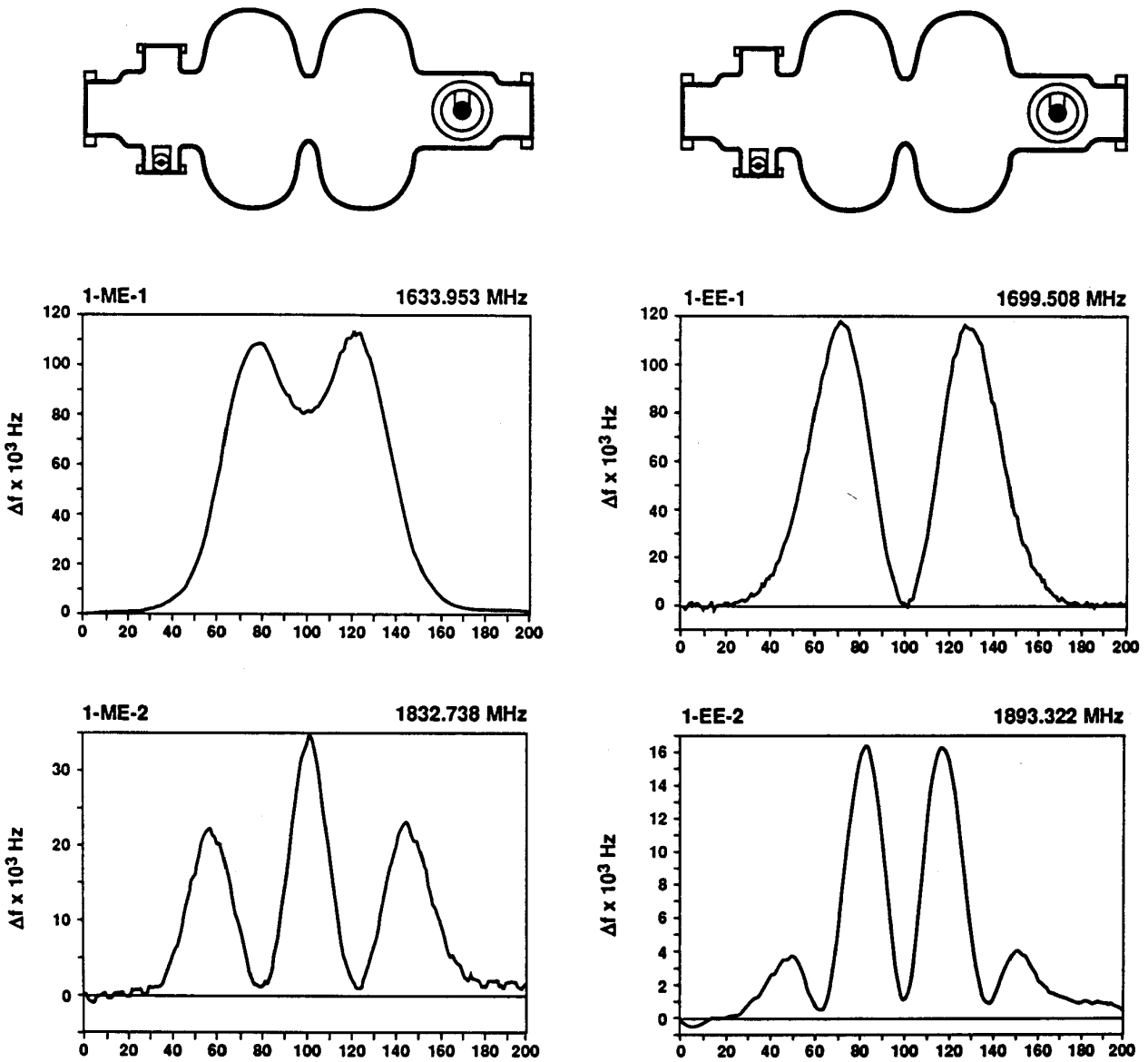## LOWEST FREQUENCY RF DIPOLE MODES

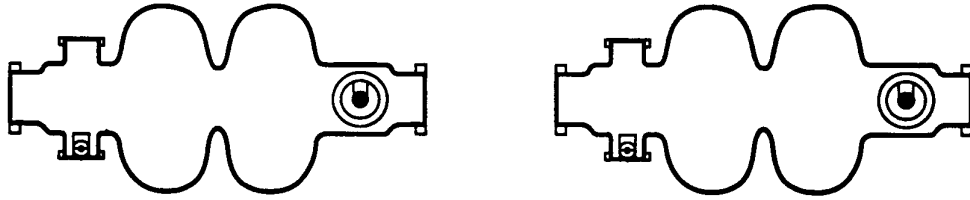Figure 4: Field profiles for the lowest frequency dipole modes.

mode, measurement noise on the field profile was too large to make a meaningful estimate of frequency difference. These results are again consistent with the expected frequency difference.

Frequency splitting of the two polarizations was observed in the "TE$_{111}$" band. The π-mode polarizations were split by 3.5 MHz and the polarization vector rotated from one end of the structure to the other. The 0-mode polarizations were split by 2 MHz and did not exhibit rotation of the polarization vector. The two polarizations in the "TM$_{110}$" band could not be resolved at a sensitivity level of < 100 kHz. The behavior of the "TM$_{110}$" band indicates that reasonable cylindrical symmetry was achieved in the cell region of the structure. The anomalous behavior of the "TE$_{111}$" band is thought to result from the coupling ports in the beam tubes, as explained in the following section.

5.2 Lowest frequency modes confined to the beam tubes.

The measured field profiles of the lowest frequency beam tube modes are presented in Figure 5. The longitudinal 0-mode and π-mode are strongly confined to the beam tubes in agreement with URMEL calculations. The very small coupling between one beam tube and the other results in significant field unflatness even for small dimensional differences. In the longitudinal modes, the field amplitude difference is over 50 percent. However, the frequency difference, calculated through a perturbation analysis, is only 2 X 10^{-4}. The coupling for the beam tube dipole modes is
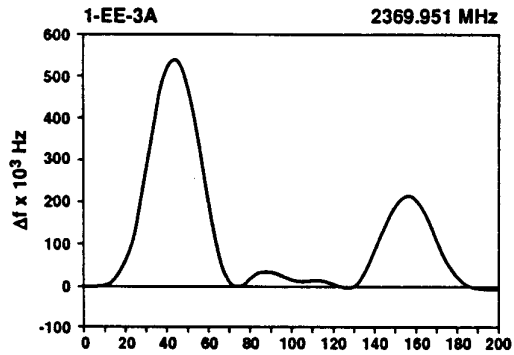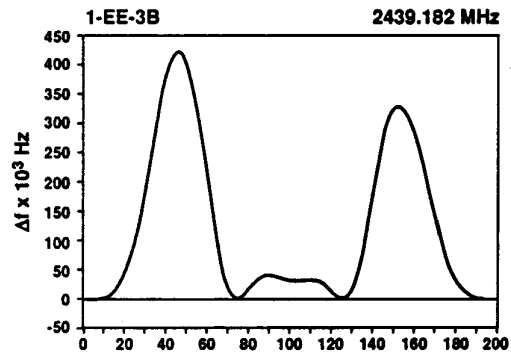
BEAM PIPE RF MODES

LONGITUDINAL
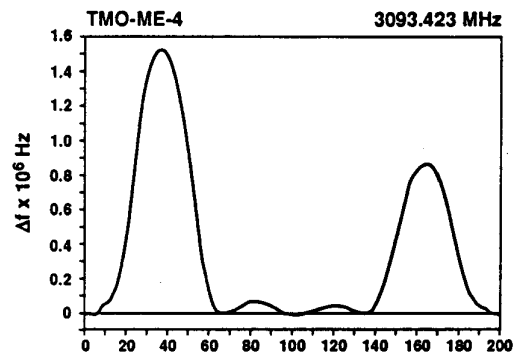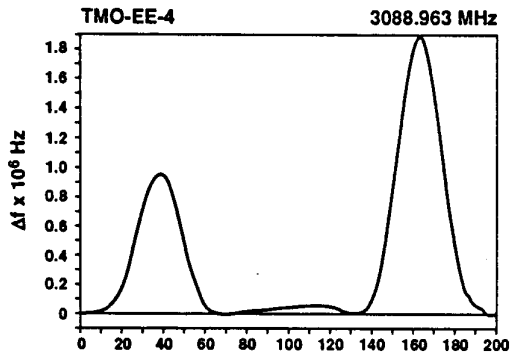
DIPOLE

Figure 5: Field profiles for the principal beam pipe modes.

also very weak. Using the same perturbation analysis, the frequency difference for these dipole modes is calculated to be a few parts in 10^{-4}. Although the beam tubes were deep drawn to achieve good dimensional control, the extremely small frequency difference observed must be partially coincidental.

In contrast to the small splitting caused by the weak coupling between beam tubes, the two polarizations of the dipole modes are split by 70 MHz due to the asymmetry introduced by the coupling ports. In each beam tube there are two coupling ports oriented directly opposite one another. However, the coupling ports in the second beam tube are rotated by 110° with respect to the ports in the first beam tube. This rotation of the ports causes the direction of the polarization vector to rotate from one end of the structure to the other as it tries to remain aligned with the ports (B polarization) or orthogonal to the ports (A polarization). This rotation of polarization is observed in these beam pipe modes and the "TE_{111}" π-mode. For the "TE_{111}" 0-mode, this rotation does not occur and the polarizations are aligned in directions that average the A and B polarizations of the beam tube modes.

5.3 Trapped dipole mode.

There is only one trapped mode below 3200 MHz in the two-cell structure. The measured field profile for this mode (1-EE-6), shown in Figure 6, confirms the URMEL prediction that the field
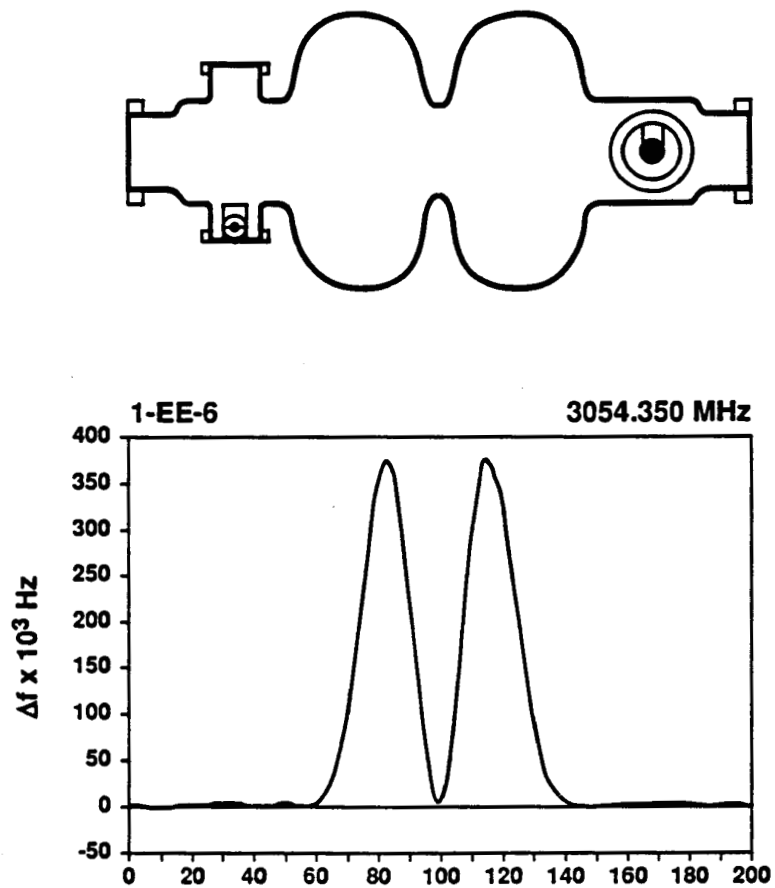
TRAPPED MODE

Figure 6: Field profile for the trapped mode.

amplitude in the beam tube is extremely small. In the cells, the field amplitude difference is 0.3 percent. Using URMEL, a frequency difference of 2×10^{-4} is calculated for this mode. The two polarizations of this mode could not be resolved. Both of these facts indicate good control over cell geometry.

6. CONCLUSIONS

The deep drawing and electron beam welding techniques used in manufacturing the structure components (dumbbells and end half-cells with beam tube) have been effective in controlling cell frequencies to within $\pm 5 \times 10^{-4}$. The use of RF measurements as a fabrication procedure that corrects frequency errors in the components makes it possible to control the cell frequencies in the accelerator mode to within $\pm 5 \times 10^{-5}$. This procedure yields a correct frequency and a flat field profile in the accelerator mode of the "as fabricated" structure, and permits partial correction of the HOMs.

7. ACKNOWLEDGMENTS

SRF91F22

8. REFERENCES

1. E.Haebel, P.Marchand, and J.Tückmantel, "An improved superconducting cavity design for LEP", Proceedings of the Second Workshop on RF Superconductivity, Part 1, pp 281-297, Geneva, Switzerland, 1984.

2. H.P.Vogel, DESY-M-85-09.

3. T.Weiland, Nucl. Instr. & Meth., 216, 1983, p.329.

4. A.Marziali, H.A.Schwettman, J.G.Hatmaker, M.W.Miller, H.G.Cambell, R. Sinko, M.W.Hamilton, C.C.Coghill, R.Dunham, J.L.Light, Carrol Allcock, "Fabrication methods of the Superconducting Injector cavities for the Stanford University Free Electron Laser", I.E.E.E. Trans. Magn., 27 (2) p1916, March 1991.

5. T.I.Smith, "Standing wave modes in a Superconducting Linear Accelerator", High Energy Physics Laboratory Report No. 437, Stanford University, Stanford, CA, 1966.